

MEMS piezoresistive flow sensors for sleep apnea therapy

Behrokh Abbasnejad^a, William Thorby^b, Amir Razmjou^d, Dayong Jin^a, Mohsen Asadnia^{b, **}, Majid Ebrahimi Warkiani^{a,c,*}



^a School of Biomedical Engineering, University of Technology Sydney, Sydney, 2007, Australia

^b School of Engineering, Macquarie University, Sydney, 2109, Australia

^d Department of Biotechnology, Faculty of Advanced Sciences and Technologies, University of Isfahan, Isfahan, 81746-73441, Iran

^c Institute of Molecular Medicine, Sechenov First Moscow State University, Moscow, 119991, Russia

ARTICLE INFO

Article history:

Received 20 February 2018

Received in revised form 6 May 2018

Accepted 17 June 2018

Available online 30 June 2018

Keywords:

Breath analyzer

MEMS flow sensor

Liquid crystal polymer

ABSTRACT

A MEMS liquid crystal polymer (LCP), used in the membrane-based pressure sensor, has been found highly useful as a flow sensor. Here we conducted a set of elaborate experiments using an air flow generator to investigate the potential of our LCP flow sensor for sleep apnea therapy. Critical properties of the LCP flow sensor, including flow range, resolution (sensitivity), accuracy, and response time, have been systematically characterized. As a result, LCP flow sensor achieves a limit of detection of 8 LPM to measure flow rate, better than the commercial flow sensor (>10 LPM). Our LCP flow sensor shows a favourable response in a large flow range (8–160 LPM) with a sensitivity of detecting a linear voltage response of 0.004 V per 1 LPM flow rate. With minimum detectable flow, high sensitivity and resolution, we further demonstrated our LCP flow sensor for detecting human respiration. Moreover, using a two-dimensional simulation in COMSOL Multiphysics, we demonstrated the deformation of LCP membrane in response to different flow velocities which leads to resistance change in sensor's strain gauge.

© 2018 Elsevier B.V. All rights reserved.

1. Introduction

The ability to accurately measure fluid flow rate is important for a variety of applications, such as environmental monitoring, process control, sensing systems in aircraft and underwater vehicles, emergency response monitoring, and in the biomedical industry [1–12]. The flow sensor is needed to regulate flow generators in the sleep apnea treatment where patients need continuous cycles of air flowing to their lungs, and to prevent a sense of stopped breathing because of a blockage (or obstruction) in the upper airway. Flow generators require sensitive flow sensors to pump accurate volume of air that is inhaled or exhaled similar to human breathing process. Conventional sensors, used to achieve this level of sensing accuracy, requires large power consumption and are large in physical size and weight, with low response and sensitivity, as they use active sensing capabilities to detect changes in fluids [13].

Flow sensors can generally be categorized into either thermal or non-thermal sensors, based on the mechanism of flow sensing. Thermal flow sensors detect the change of thermal energy when fluid flow is interacting with a hot body [14]. The high power consumption and less compliance to integration with other microstructures are the disadvantages of the thermal flow sensors. In the recent years, research has been concentrated on developing non-thermal flow sensors, including piezoelectric [15] and piezoresistive [16] flow sensor. Most of the non-thermal flow sensors detect the pressure change as a function of resistance or capacitance changes when a fluid flows over the surface of the sensor.

Common issues associated with Microelectromechanical systems (MEMS) based flow sensors include the lack of repeatability and sensitivity, as a bottleneck reducing their practical applications. Research has found that there is an observed trade-off between the mechanical strength and reliability of the device against its sensitivity [13] largely due to the inconsistency of fabrication process and material selection. Hence the structural material plays an important role in sensing capability of a flow sensor. Silicon is one of the frequently used structural material for air flow sensing. However, for this application, silicon has some limitations such as low mechanical yield strain, with insufficient sensitivity to measure the large fluctuation of the flow [17–19]. Using Liquid-crystal polymers (LCP) in device fabrication could potentially solve these issues in developing MEMS flow sensors. Our group has developed

* Corresponding author at: School of Engineering, Macquarie University, Sydney, 2109, Australia.

** Corresponding author.

E-mail addresses: Behrokh.AbbasnejadTalebkhani@student.uts.edu.au (B. Abbasnejad), William.Thorby@mq.edu.au (W. Thorby), amir.razmjouchaharmahali@mq.edu.au (A. Razmjou), Dayong.Jin@uts.edu.au (D. Jin), mohsen.asadnia@mq.edu.au (M. Asadnia), Majid.Warkiani@uts.edu.au (M. Ebrahimi Warkiani).

several MEMS piezoelectric and piezoresistive flow sensors for various applications [20–23], including a miniaturized piezoresistive LCP sensor for underwater sensing [24]. The sensor we used in this study is made of an LCP membrane with much higher sensitivity over silicon as a structural material for flow sensing and better flexibility, as its Young's modulus (2.16 GPa) is much lower than silicon (185 GPa) [25]. Moreover, LCP is highly resistant to chemicals and has a very low moisture absorption capability, which makes the sensor robust for applications in harsh environments [13].

The purpose of this study is to analyze the critical properties of our LCP membrane-based flow sensor using an airflow generator for sleep apnea application. For this purpose, we have investigated the following parameters: flow range, resolution (sensitivity), accuracy, and response time for both LCP sensor and the commercial sensor. To show an overview of the LCP flow sensor response, we have plotted the calibration diagram of the LCP flow sensor based on experimental results. Also, the sensor has been tested for responding to calm human breathing and the inhalation and exhalation individually.

2. Sensor design and fabrication

The fabrication process has been described in our previous study [22]. Briefly, the four major fabrication steps include LCP silicon wafer bonding, deep reactive-ion etching (DRIE) for through-hole formation, sputtering a metal resistor and lift-off for resistor pat-

ternning. This fabrication process under low-temperature ($<130^{\circ}\text{C}$) employment is simple, low-cost, and repeatable. The schematic of all four steps of the fabrication process is shown in Fig. 1a–d. The device fabrication begins with etching the copper-cladding completely from both sides of a 25 μm thick LCP (3908) film. The next step is bonding the LCP and silicon by using an SU-8 intermediate adhesion layer. Instead of direct bonding, the intermediate SU-8 adhesion layer is used for bonding to avoid the buckling which occurred due to a large mismatch between the thermal coefficient of silicon ($3.2 \text{ ppm } ^{\circ}\text{C}^{-1}$) and LCP ($18 \text{ ppm } ^{\circ}\text{C}^{-1}$).

Beforehand spin coating SU-8, the silicon wafer was cleaned in a piranha solution to avoid particle contamination then dehydrated on a hotplate at 130°C for 20 min to improve the adhesion of an SU-8 layer. The SU-8 2002 is spin coated at 2500 rpm for 30 s on a silicon wafer to form a 5 μm thick layer. An LCP film cut into the shape of the silicon wafer was carefully placed and pressed with uniform pressure on the silicon wafer to ensure that no air bubbles are trapped in between. This wafer-pair was heat treated to harden the SU-8 layer and eventually, enhance the bond strength. During the heating process, a uniform pressure was applied by placing uniform circular metal wafers on the bonded wafer-pair. The wafer-pair was heat treated in three steps and temperature was increased in each step starting at 45°C for 20 min, then at 80°C for 10 min followed by 120°C for 20 min.

The LCP diaphragm was released by etching DRIE holes on the silicon side of the bonded wafer-pair as shown in Fig. 1b. During

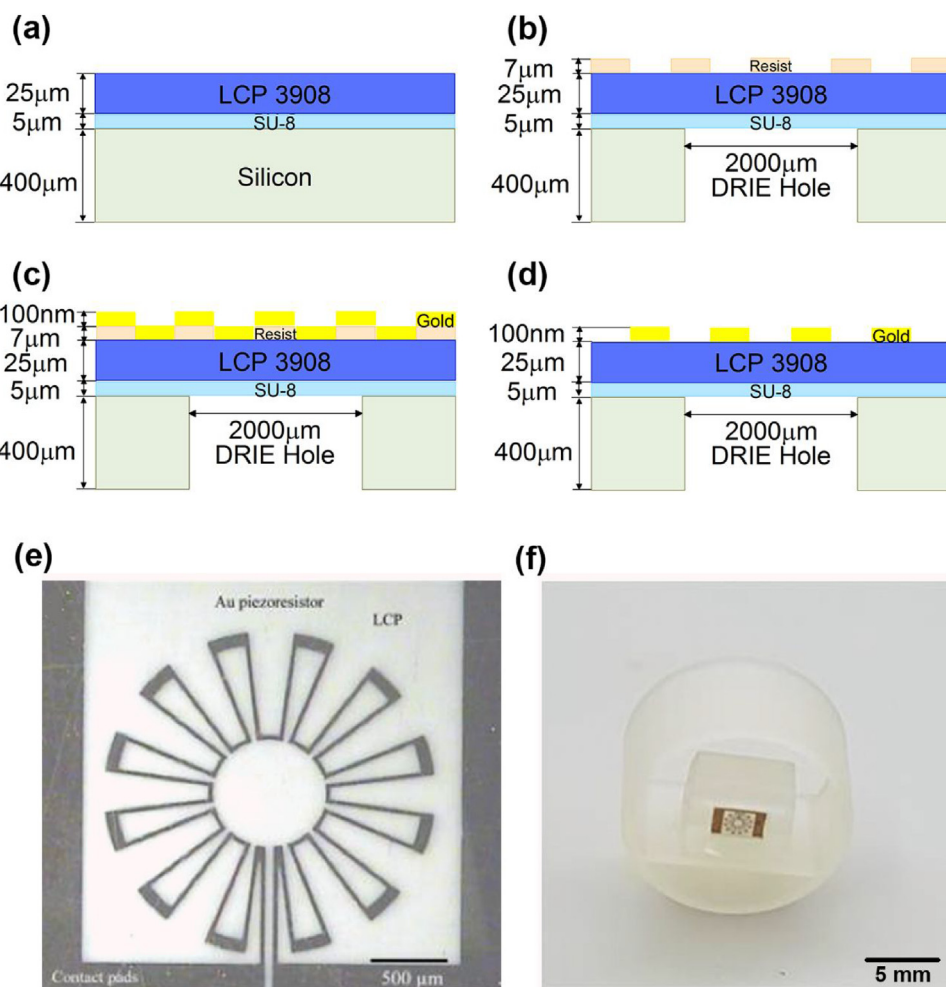


Fig. 1. Overview of the fabrication process for the LCP flow sensor: (a) LCP–silicon bonding with an SU-8 intermediate layer, (b) DRIE etching 400 μm through-hole and resist patterning, (c) 100 nm gold sputter deposition and (d) gold lift-off. (e) Optical image of the LCP flow sensor after fabrication [13] (f) 3D printed housing to package the sensor in flow generator tube.

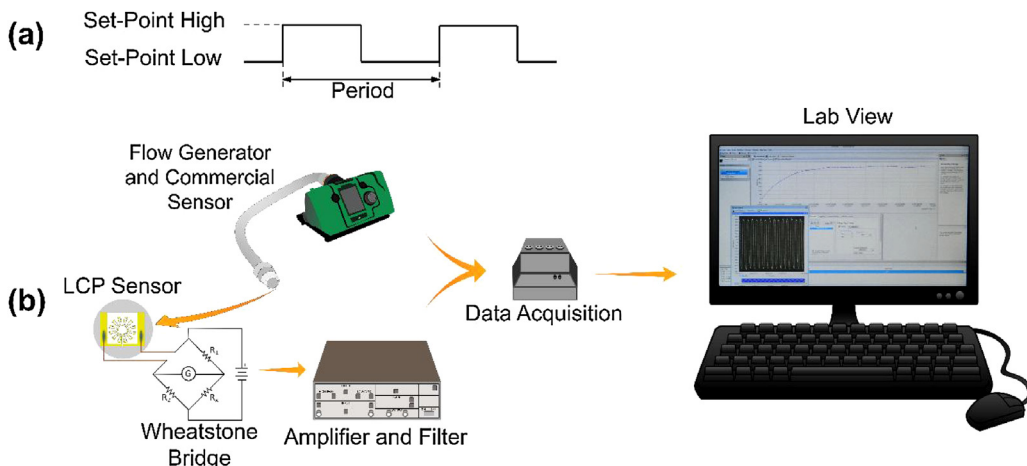


Fig. 2. (a) Flow pattern generated by the flow generator that mimics exhalation (b) Schematic cartoon shows the experimental setup which depicts how LCP flow sensor is connected to the flow generator, filter/ amplifier and data acquisition devices.

the DRIE etching, a protection silicon wafer spin-coated with 5 μm resist was bonded to the LCP side of the wafer pair to protect the LCP film.

After etching DRIE holes, it is easy to remove this protection wafer by dipping in acetone for a few minutes while the bonding remains intact. In the next step, the thin film resistor was formed on the diaphragm surface. Au was chosen as the strain gauge because of its high gauge factor and more conformal deposition than other metals. The LCP membrane has uniform thickness because it is not defined by an etching process.

Afterwards, a 7 μm thick resist was spin-coated on the LCP membrane for lift-off process. The resist was patterned by a mask containing the serpentine resistor features aligned with the DRIE holes using backside alignment as shown in Fig. 1b. Then, a 100 nm Au layer (with a 10 nm Cr layer to enhance Au adhesion) was sputter deposited on the patterned resist as shown in Fig. 1c. The last step is to lift off the Au by removing the sacrificial resist layer by dipping the wafer in an ultrasonically agitated acetone solution for 20 s.

3. Sensor structure and sensing principle

As mentioned in the previous section, the piezoresistive LCP flow sensor is originally a micro diaphragm device consisted of a 25 μm thick liquid crystal polymer (LCP) circular sensing membrane with a diameter of 2000 μm . 100 nm thick Gold strain gauges with a serpentine shape are deposited on the periphery of the LCP membrane where maximum stress is generated due to air pressure on the membrane. To position the sensor at the end of the flow generator's tube, a circular housing which can accommodate the tube was 3D printed. The 3D printed housing has a special part for the LCP sensor which the plane of the sensor membrane would be perpendicular to the plane of the airflow direction in the tube. The LCP was bonded to the housing inner part surface using nonconductive epoxy. Fig. 1e and f show the optical image of the sensor, and the 3D printed housing with the sensor mounted on it.

4. Flow sensing characterization

For characterization analysis of our LCP MEMS flow sensor, a set of experiments conducted to test the device. The LCP sensor, located at the end of the flexible tube attached to a continuous positive airway pressure (CPAP) machine/flow generator used for the sleep apnea treatment. There was a commercial sensor available inside the flow generator machine to sense the air flow continu-

ously which was directly connected to National Instruments data acquisition (NI-DAQ) system cDAQ 9174 series (National instrument, Texas, U.S.). The LCP sensor was connected to an external Wheatstone bridge biased with 5 V and connected to an amplifier and filter with a gain of 50 and a 3 Hz low pass filter. The output signal from the amplifier/low pass filter system was then used as inputs into the NI-DAQ. Data was then captured and recorded in National Instruments Signal Express 2015 software, where 1000 samples were taken at a rate of 2 kHz.

As shown in Fig. 2a, the flow generator used in the experiments has three main parameters which are set-point high (SLMP), set-point low (SLMP), and period (ms). These steps allow the flow generator to mimic the cycle of human breathing. All experiments were conducted using the air flow generator default period of 3000 ms. Value of 'set high point' varied from 20LMP to 200 LMP, and 'set low point' was kept at a constant value of 0 LPM.

Fig. 2b shows a schematic of the experimental setup. The sensor was located at the end of the pipe of the fluid generator with the plane of the sensor membrane perpendicular to the plane of the airflow direction. The generated air velocity was increased step by step while the resistance change data from the sensor were continuous.

5. Results

A set of experiments are conducted in order to analyze the LCP flow sensor characteristics. The main focus of study for these experiments are the flow ranges, resolution, and accuracy and response time of the LCP sensor which are critical for sleep apnea therapy. An air flow generator was used to test the system response to air flow velocities as well as using the commercially available sensor built into the flow generator for a direct comparison of key performance measures.

5.1. Simulation

Finite element analyses were conducted on COMSOL Multiphysics to investigate the fluid-flow interaction with the sensor's diaphragm and the response of the sensor to various airflow velocities from air flow generator used for sleep apnea therapy.

This simulation gives valuable information about sensor housing design. In order to acquire the maximum sensitivity, the housing must allow the LCP sensor to be subjected to maximum membrane displacement. From the simulation, we can see that the sensor is required to face perpendicular to the direction of the fluid flow, which will make the sensor's membrane deflect with maxi-

Table 1

Mechanical properties of SU-8 and LCP used in simulations.

Layer	Young's modulus (GPa)	Poisson ratio	Thickness (μ)	Reference
LCP	2.1	0.3	25	[26]
SU-8	4.1	0.22	5	[27]

mum displacement at each varying flow rate. The placement of the sensor is required to be as close to the centre of the pipe as possible due to viscosity on laminar flow and friction caused with the interaction of the inner walls and laminar flow, creating a boundary layer extending from the walls. Furthermore, taking into consideration the ease of assembly, the sensor position is slightly lower than the exact centre of the tube, although not at the exact centre of the tube, this position was still above the boundary layer created.

Since a thin layer of SU-8 (5 μ m) was used to bond the LCP layer (25 μ m) to the silicon substrate, both these layers were considered in defining the sensor's diaphragm in the finite element analysis simulations. **Table 1** shows the values of Young's modulus, Poisson ratio and thickness, which were applied for the LCP layer and SU-8 in the simulation. Although the SU-8 layer is critical for bonding the LCP layer to silicon, it creates a stiffer diaphragm, which affects the sensor sensitivity. Nevertheless, our experimental results revealed that the sensitivity of the sensors with SU-layer is sufficient to use the device in the flow generator for sleep apnea application. There are different methods of photoresist patterning to selectively form the SU-8 on the LCP membrane to avoid covering the diaphragm which will increase the sensitivity of the sensor.

The simulation was conducted for air flow range of 20 LPM to 200 LPM in accordance with the flow range we used for collecting the experimental data.

Fig. 3a shows the simulation results with housing and sensor located at the end of flow generator's tube (10 cm in length) in order

to replicate the length of the tube attached to the CPAP device. **Fig. 3c and d** shows the deformation and stress applied by the air flow to the membrane at its given velocity.

Fig. 3b shows the membrane displacement results from applying a parametric sweep to the flow velocity at the inlet of the simulation to replicate different flow rates generated by the CPAP device. Based on the simulation of membrane displacement, there is distinct, measurable membrane displacement for each 10 LPM flow rate step and by increasing the fluid flow velocity, the displacement of the membrane will increase.

The difference in maximum displacement of the membrane increases nonlinearly with flow rate, indicating that the difference in sensitivity may be difficult to distinguish at lower flow velocity changes compared to higher flow rate changes.

5.2. Flow range characterization

Since the primary goal of this paper is to investigate the performance of our MEMS LCP sensor in flow generators used for the sleep apnea treatment, it is critical to ensure the sensors can function in the range of minimum and maximum inhalation or exhalation pressure magnitude. From our experiments, the maximum air flow during normal respiration is 60 LPM while this value increases to 120 LPM during exercising. **Fig. 4** shows an overview of the results from the experiments performed and recorded from LCP and commercial sensors outputs ranging from 10 to 200 LPM. **Fig. 4a** revealed that increasing the air flow will cause an increase in the sensor output. The more the fluid flow generated by the fluid generator, the more the sensor output as a voltage until 160 LPM and this fact is in accordance with the simulation result. As it can be seen from **Fig. 4a**, The LCP sensor output increases uniformly with respect to air flow up to 160 LPM and afterwards the increment value does not follow the trend. This might be due to the saturation of sensors which occurs as higher flow rates limit LCP micro

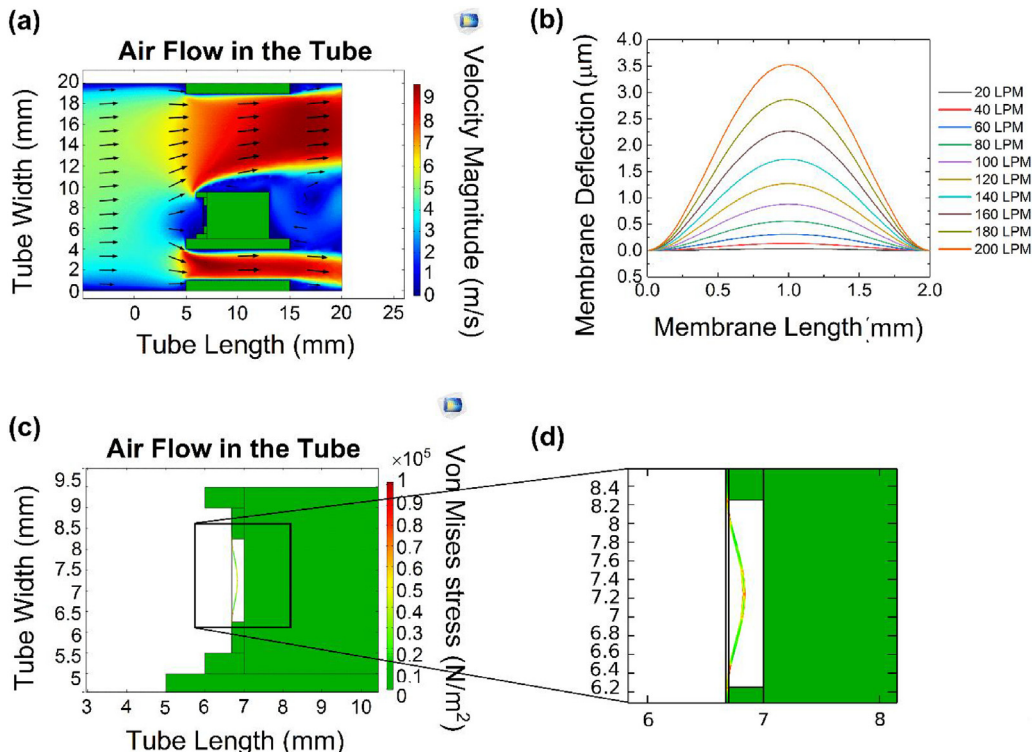


Fig. 3. Simulation results of the LCP sensor with COMSOL Multiphysics software. (a) Fluid flow distribution in the flow generator tube, (b) LCP sensor membrane deflection along the membrane for various flow input (c) the close-up view of the LCP membrane deflection and (d) A large-scale display of the selected part of the previous LCP membrane deflection graph.

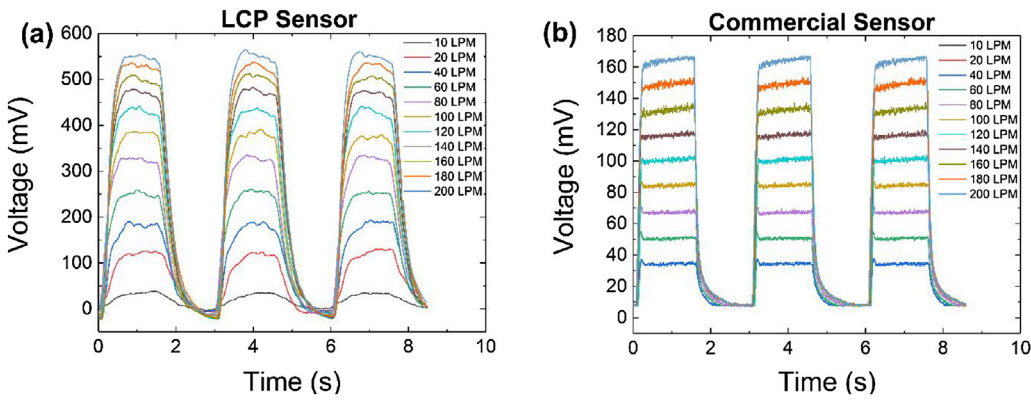


Fig. 4. Flow sensing range overview (a) LCP sensor, (b) Commercial flow sensor inside the flow generator.

diaphragm bending due to its elastic properties. Thus, the reliable maximum flow rate detectable by LCP sensor is 160 LPM. However, since the maximum air flow generated in respiratory systems is about 120LMP, this value is sufficient for sleep apnea and breathalyzer devices. In the breath analysing applications, since human breath temperature is about 37 °C, the effect of temperature change in sensor performance needs to be considered. However, in this work, since the sensor is mounted at the end of the flow generator tubing, which is about 50 cm long, it is safe to consider the sensor is exposed to flow at room temperature.

Fig. 5a depicts the calibration plot of the LCP sensor in terms of peak-to-peak sensor output as a function of air flow generated. In this figure, the graphed points represent the average peak-to-peak voltages gathered from 4 to 5 periods of air flow, with error bars giving the standard deviation of these results. As can be seen from the Fig. 5a, when fitting a linear line of best fit, we can see that for voltage increase by 0.004 V for every 1 LPM increase in flow rate.

Experimentation was also conducted to observe the low flow rate detection capabilities of the LCP sensor in comparison with the commercial sensor. Fig. 5b shows that the LCP sensor was able to demonstrate clear sensing capabilities at flow rates as low as 8 LPM where the lowest detectable flow rate of the commercial sensor inside the flow generator is 10 LPM.

5.3. Resolution analyses

For investigating the resolution and sensitivity of the LCP flow sensor, a set of experiments were conducted to determine if there was a measurable difference between flow rates at 1 LPM intervals

at various flow rates. Fig. 6 and 7 show the flow ranges of 8–10 LPM, 97–100 LPM, and 197–200 LPM for both LCP and commercial flow sensor. According to the Fig. 6, the LCP sensor demonstrates a measurable resolution of 1 LPM from all flow rates tested from 8 to 200 LPM. To be able to compare the LCP flow sensor's resolution results with the Commercial sensor, the average pick-to-peak voltage of both sensors are listed in Table 2.

5.4. Band gap/response time

The response time of the sensor is defined as the interval required by the output signal of the sensor to display a stable change in applied air flow. This value is especially important for the high-frequency application to ensure a stable output signal can be observed at each stimulus. The typical respiratory rate for healthy adults at rest is 12–18 breath per minutes which is considered a very low frequency and easily detectable for our LCP sensors. Throughout the experiments, we studied the response time of LCP and commercial sensor to determine how fast the LCP will reach a stable value during the breathing process. The response time of the LCP sensor graphically is shown in Fig. 8.

The response times on average for the LCP MEMS sensor is 0.6 s as listed in Table 3. Using a polymer as the membrane material, the sensor itself require time for the membrane to undergo deformation in response to the change in air pressure; in order for a resistance to be applied, the sensor must undergo mechanical stress in the flexible membrane which requires time for the maximum stress to be applied at each respective flow rate; as the flow rate increases the faster the response time. Here, by comparing the

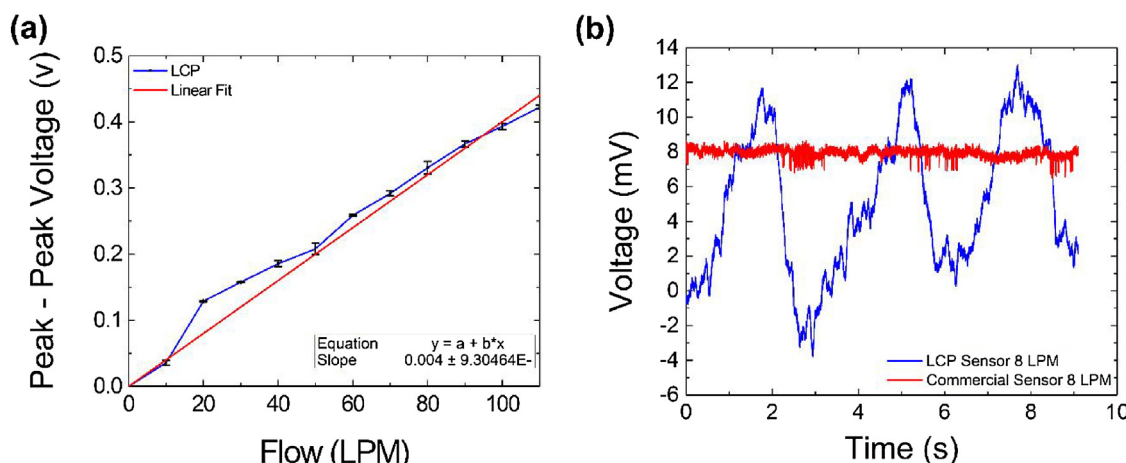


Fig. 5. (a) Calibration Plot for LCP flow sensor (b) The comparison of the LCP flow sensor response with commercial one for low detectable flow rate 8 LPM.

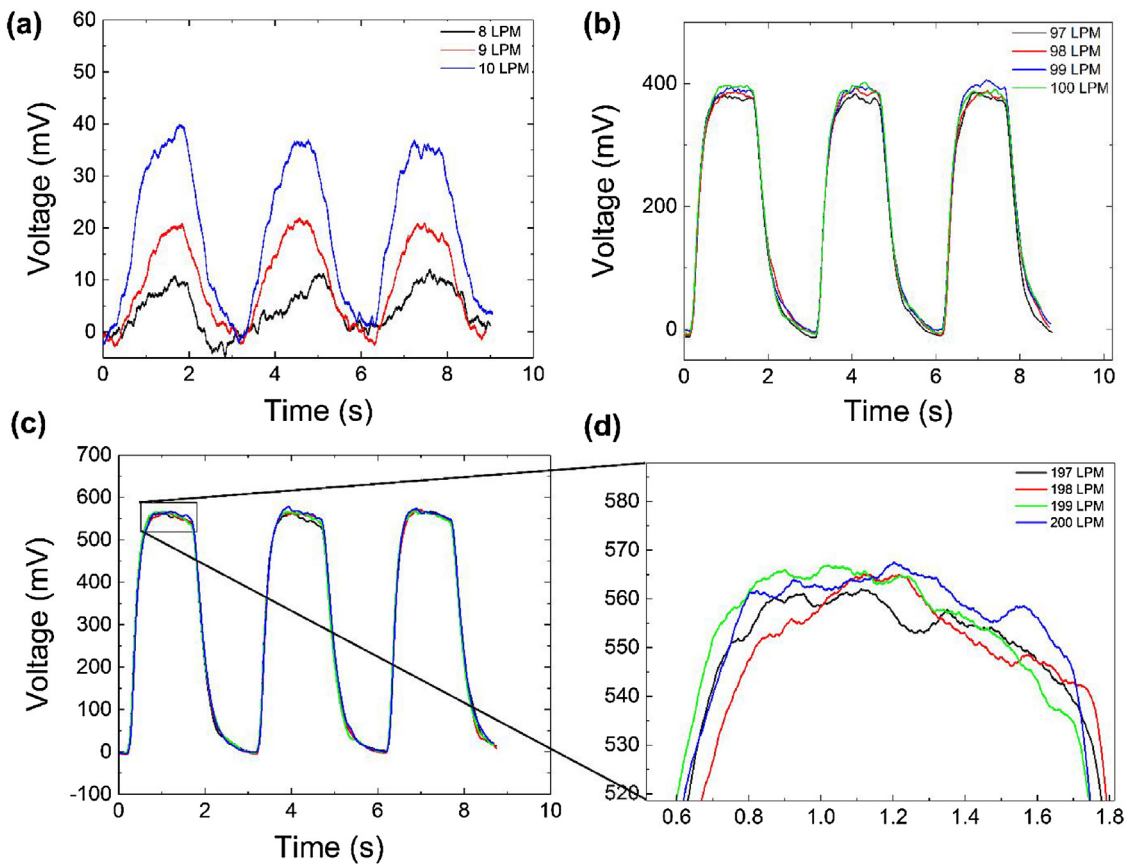


Fig. 6. Sensitivity and resolution of the LCP flow sensor (a) 8–10 LPM (b) 97–100 LPM, and (c) 197–200 LPM (d) A large-scale display of the selected part of the previous 197–200 LPM resolution graph.

Table 2
Average Pick-To-Peak Voltage for LCP and Commercial Sensors.

Flow Rate (LPM)	Peak-to-Peak LCP Sensor Output (mV)	Reference Figure	Peak-to-Peak Commercial Sensor Output (mV)	Reference Figure
8	0.0141	6a	N/A	7a
9	0.0240	6a	0.0026	7a
10	0.0386	6a	0.0032	7a
97	0.3952	6b	0.0748	7b
98	0.3989	6b	0.0759	7b
99	0.4015	6b	0.0770	7b
100	0.4020	6b	0.0778	7b
197	0.5641	6c-6d	0.1536	7c-7d
198	0.5689	6c-6d	0.1567	7c-7d
199	0.5701	6c-6d	0.1574	7c-7d
200	0.5747	6c-6d	0.1580	7c-7d

Table 3
Response Time Comparison.

Flow Rate (LPM)	LCP MEMS Sensor Response Time (s)	Commercial Sensor Response Time (s)
10	1	N/A
50	0.6	0.15
100	0.6	0.1
150	0.6	0.1
200	0.6	0.1

response time of both LCP and commercial sensor, it is clear that the response time for the commercial sensor is smaller than that of LCP sensor. Although having lower response time does limit the applicability of LCP sensors in respiratory systems, this parameter can be improved by enhancing the bonding (LCP to the substrate), using a thicker LCP membrane or an alternative material for LCP membrane with higher Young's module.

5.5. Application: human breath monitoring system

Testing was also conducted to determine if the sensor would respond to the air flow changes generated from the human respiratory system, determining the inspiratory flow profile and inhalation to exhalation ratio is an important study in the clinical field. It can be used for controlling the pressure and flow rate of a respiratory gas delivered to a patient and monitoring the patient's breathing [28–30].

Fig. 9 below shows the response given by testing the LCP sensor to calm human breathing as well as inhalation and exhalation individually. As it can be seen from the Fig. 9a, the sensor is able to detect and respond very well to airflow to the calm action of human respiratory, the positive air flow created from exhaling and the negative air flow created from inhaling. The response from inhaling is noticeably larger than the response from exhaling. This is due to the material properties of the LCP membrane in the piezoresis-

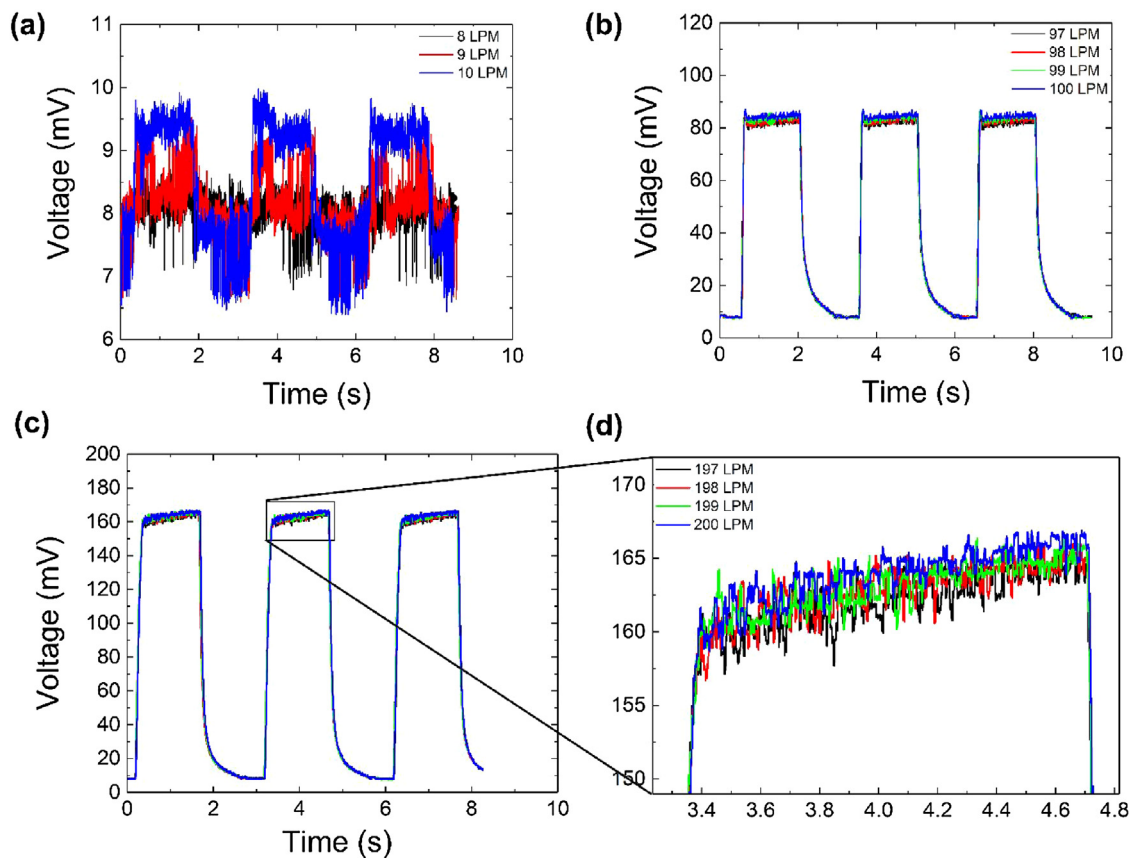


Fig. 7. Sensitivity and resolution of the commercial flow sensor (a) 8–10 LPM (b) 97–100 LPM, and (c) 197–200 LPM (d) A large-scale display of the selected part of the previous 197–200 LPM resolution graph.

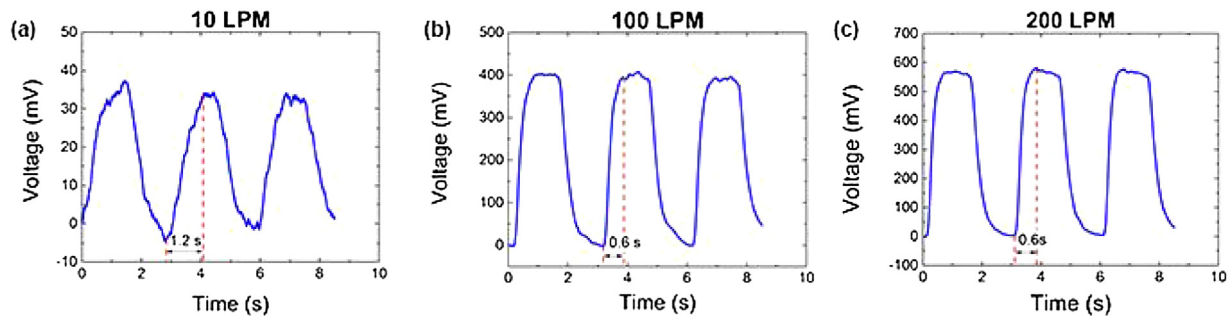


Fig. 8. The response time for the LCP flow sensor (a) 10 LPM, (b) 100 LPM, and (c) 200 LPM.

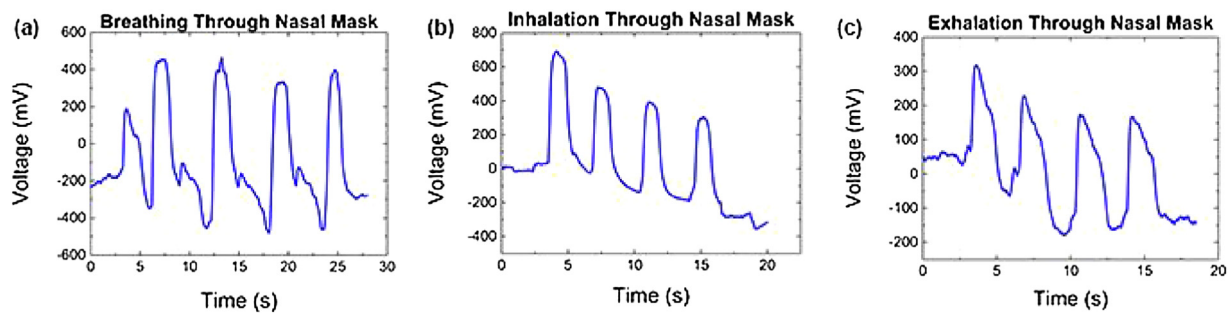


Fig. 9. The LCP flow sensor for human respiratory flow rate (a) breathing, (b) Inhalation, and (c) Exhalation.

tive sensor, as previously mentioned, the material in the LCP sensor require time to rectify deformation that occurs due to air flow velocity, it can be hypothesised that maximum strain has occurred upon

inhaling and therefore when exhaling immediately after, the sensor has not been given enough time to rectify deformation that has occurred during inhaling and thus the sensor has not returned to

its normal state to respond to the exhale portion of the breathing cycle. On the other hand, it is demonstrated that the flow rate during inhalation is much higher than exhalation period [31].

6. Conclusion

Elaborate characterization and testing results of the LCP sensor as an airflow rate sensor have been presented. A number of tests have been conducted to analyze the properties of the LCP MEMS flow sensor. The main focus of study for these experiments has been at the flow ranges, resolution, accuracy and response time of the LCP sensor. It is shown that the sensor is capable of detecting air flow rates from 10 to 200 LPM and even as low as 8 LPM. The fact of increasing fluid flow rate causes an increase in the deformation of the membrane is verified by simulation done by COMSOL. The calibration curve of the sensor based on experimental results is plotted, and the relation between flow rate and the output voltage of the sensor is shown. Average voltage response of 0.004 V per 1 LPM flow rate change with an average standard deviation of 0.0047 across flow rates of 10–200 LPM is shown on the calibration curve. For testing the resolution of the LCP flow sensor, it is demonstrated that there is a measurable difference of 1 LPM changes at various flow rates. In order to examine the accuracy of the flow sensor, the average response time of the LCP flow sensor is 0.6 s. Because the LCP membrane has a low Young's modulus, it is flexible. Even though, this flexibility of the LCP will help the sensor to be much more sensitive; the response time will be higher. Finally, it is shown that the LCP MEMS flow sensor is able to detect respiratory system response from inhalation and exhalation.

Conflict of interest

The authors declare that there is no conflict of interest regarding the publication of this paper.

Acknowledgment

This work was supported by the Australian Research Council Centre Discovery Early Career Researcher Award (DECRA) DE180100688. The authors would like to thank Dr Ajay Giri Prakash Kottapalli for his contribution in the device fabrication.

References

- [1] D.J. Apigo, P.L. Bartholomew, T. Russell, A. Kanwal, R.C. Farrow, G.A. Thomas, An angstrom-sensitive, differential MEMS capacitor for monitoring the milliliter dynamics of fluids, *Sens. Actuators A Phys.* 251 (2016) 234–240.
- [2] M. Asadnia, A.G. Kottapalli, R. Haghghi, A. Cloitre, P.V. Alvarado, J. Miao, M. Triantafyllou, MEMS sensors for assessing flow-related control of an underwater biomimetic robotic stingray, *Bioinspir. Biomim.* 10 (3) (2015) 036008.
- [3] A. Baldwin, L. Yu, E. Meng, An electrochemical impedance-based thermal flow sensor for physiological fluids, *J. Microelectromech. Syst.* 25 (6) (2016) 1015–1024.
- [4] B.W. Bequette, *Process Control: Modeling, Design, and Simulation*, Prentice Hall Professional, 2003.
- [5] J.A. Ellis, M. Banu, S.S. Hossain, R. Singh-Moon, S.D. Lavine, J.N. Bruce, S. Joshi, Reassessing the role of intra-arterial drug delivery for glioblastoma multiforme treatment, *J. Drug Deliv.* 2015 (2015) 15.
- [6] E. Ghafar-Zadeh, B. Gholamzadeh, G. Alyala-Charca, P.B. Raveri, M. Matynia, M. Sawan, F. Awwad, S. Magierowski, Toward spirometry-on-chip: design, implementation and experimental results, *Microsyst. Technol.* 23 (10) (2016) 4591–4598.
- [7] W. Iwasaki, H. Nogami, H. Ito, T. Gotanda, Y. Peng, S. Takeuchi, M. Furue, E. Higurashi, R. Sawada, Useful method to monitor the physiological effects of alcohol ingestion by combination of micro-integrated laser doppler blood flow meter and arm-raising test, *Proc. Inst. Mech. Eng.* 226 (10) (2012) 759–765.
- [8] W. Iwasaki, H. Nogami, S. Takeuchi, M. Furue, E. Higurashi, R. Sawada, Detection of site-specific blood flow variation in humans during running by a wearable laser doppler flowmeter, *Sensors (Basel)* 15 (10) (2015) 25507–25519.

- [9] C.-Y. Lee, C.-C. Shen, F.-H. Liu, Y.-M. Chang, In-situ monitoring of temperature, flow and pressure in micro methanol reformer by embedded integrated multifunction micro sensor, *Int. J. Electrochem. Sci.* 8 (2013) 5817–5827.
- [10] C. Malone, T. Larson, G. Simon, Thermal and power management apparatus. In Google Patents: 2005.
- [11] H. Qu, CMOS MEMS fabrication technologies and devices, *Micromachines* (2) (2016) 7.
- [12] C.-L. Wei, C.-F. Lin, I.T. Tseng, A novel MEMS respiratory flow sensor, *IEEE Sens. J.* 10 (1) (2010) 16–18.
- [13] A.G.P. Kottapalli, C.W. Tan, M. Olfatnia, J.M. Miao, G. Barbastathis, M. Triantafyllou, A liquid crystal polymer membrane MEMS sensor for flow rate and flow direction sensing applications, *J. Micromech. Microeng.* 21 (8) (2011), 085006.
- [14] J.T.W. Kuo, L. Yu, E. Meng, Micromachined thermal flow sensors—a review, *Micromachines* 3 (4) (2012) 550–573.
- [15] W.-Y. Chang, C.-H. Chu, Y.-C. Lin, A flexible piezoelectric sensor for microfluidic applications using polyvinylidene fluoride, *IEEE Sens. J.* 8 (5) (2008) 495–500.
- [16] Z. Fan, J. Chen, J. Zou, D. Bullen, C. Liu, F. Delcomyn, Design and fabrication of artificial lateral line flow sensors, *J. Micromech. Microeng.* 12 (5) (2002) 655.
- [17] T. Neda, K. Nakamura, T. Takumi, A polysilicon flow sensor for gas flow meters, *Sens. Actuator A: Phys.* 54 (1–3) (1996) 626–631.
- [18] Y. Su, A. Evans, A. Brunschweiler, G. Ensell, Characterization of a highly sensitive ultra-thin piezoresistive silicon cantilever probe and its application in gas flow velocity sensing, *J. Micromech. Microeng.* 12 (6) (2002) 780.
- [19] Y.-H. Wang, C.-Y. Lee, C.-M. Chiang, A MEMS-based air flow sensor with a free-standing micro-cantilever structure, *Sensors* 7 (10) (2007) 2389–2401.
- [20] M. Asadnia, A.G.P. Kottapalli, R. Haghghi, A.Y. Cloitre, P.V. Alvarado, J. Miao, M. Triantafyllou, MEMS sensors for assessing flow-related control of an underwater biomimetic robotic stingray, *Bioinspir. Biomim.* 10 (3) (2015), 036008.
- [21] M. Asadnia, A.G.P. Kottapalli, K.D. Karavatiki, M.E. Warkiani, J. Miao, D.P. Corey, M. Triantafyllou, From biological cilia to artificial flow sensors: biomimetic soft polymer nanosensors with high sensing performance, *Sci. Rep.* 6 (2016) 32955.
- [22] A.G.P. Kottapalli, M. Asadnia, J. Miao, M. Triantafyllou, Touch at a distance sensing: lateral-line inspired MEMS flow sensors, *Bioinspir. Biomim.* 9 (4) (2014), 046011.
- [23] A.G.P. Kottapalli, M. Bora, M. Asadnia, J. Miao, S.S. Venkatraman, M. Triantafyllou, Nanofibril scaffold assisted MEMS artificial hydrogel neuromasts for enhanced sensitivity flow sensing, *Sci. Rep.* 6 (2016) 19336.
- [24] A.P. Kottapalli, M. Asadnia, J. Miao, M. Triantafyllou, In electrosprayed nanofibers encapsulated in hydrogel cupula for biomimetic MEMS flow sensor development, micro electro mechanical systems (MEMS), in: 2013 IEEE 26th International Conference on IEEE, 2013, pp. 25–28.
- [25] J. Thaysen, A.D. Yalcinkaya, P. Vettiger, A. Menon, Polymer-based stress sensor with integrated readout, *J. Phys. D Appl. Phys.* 35 (21) (2002) 2698.
- [26] A.G. Kottapalli, M. Asadnia, J. Miao, G. Barbastathis, M.S. Triantafyllou, A flexible liquid crystal polymer MEMS pressure sensor array for fish-like underwater sensing, *Smart Mater. Struct.* 21 (11) (2012), 115030.
- [27] T.G. Xu, J.H. Yoo, S. Babu, S. Roy, J.B. Lee, H.B. Lu, Characterization of the mechanical behavior of SU-8 at microscale by viscoelastic analysis, *J. Micromech. Microeng.* (10) (2016) 26.
- [28] M.C. Pastor, F.J. Menéndez, M.T. Sanz, E.V. Abad, The influence of respiration on biofeedback techniques, *Appl. Psychophys. Biofeedback* 33 (1) (2008) 49–54.
- [29] A. Stewart, N. Finer, K. Peters, Effects of alterations of inspiratory and expiratory pressures and Inspiratory/Expiratory ratios on mean airway pressure, blood gases, and intracranial pressure, *Pediatrics* 67 (4) (1981) 474–481.
- [30] I. Van Diest, K. Verstappen, A.E. Aubert, D. Widjaja, D. Vansteenkiste, E. Vlemincx, Inhalation/exhalation ratio modulates the effect of slow breathing on heart rate variability and relaxation, *Appl. Psychophys. Biofeedback* 39 (3–4) (2014) 171–180.
- [31] B. Sul, A. Wallqvist, M.J. Morris, J. Reifman, V. Rakesh, A computational study of the respiratory airflow characteristics in normal and obstructed human airways, *Comput. Biol. Med.* 52 (2014) 130–143.

Biographies

Behrokh Abbasnejad is a Ph.D. candidate in the School of Biomedical Engineering at UTS and recipient of the prestigious Australian Government Research Training Program Scholarship (2016). She received both her B.Sc. and M.Sc. degree in Mechanical Engineering (Applied Design) from Urmia University, Iran. Her research interests include biomimetics, bio-inspired MEMS/NEMS sensors, and additive manufacturing. She is currently working on Biomimetic Flow Sensors and their applications in inner ear.

William Thorby is an undergraduate student in mechatronic at Macquarie university. His undergraduate thesis is on testing and characterising MEMS sensors.

Amir Razmjou received his PhD from University of New South Wales in 2015. He currently works at the Advance Sciences and Technologies, University of Isfahan. Amir does research in Chemical Engineering, Nanotechnology and Polymer Chemistry. Their current project is 'The Superhydrophobic Modification on the Alu-

minum Surface to Study Biological interaction: Protein Adsorption and Bacterial Attachment.

Dayong Jin Distinguished Professor Dayong Jin is a former ISAC scholar (awarded in 2007). He directs the Australian Research Council IDEAL Research Hub and Institute for Biomedical Materials & Devices (IBMD), at the University of Technology Sydney. His research has been in the physical, engineering and interdisciplinary sciences. He is a technology developer with expertise covering optics, luminescent materials, sensing, automation devices, microscopy imaging, and analytical chemistry to enable rapid detection of cells and molecules and engineering of sensors and photonics devices. Prof Jin is the winner of the Australian Museum Eureka Prize for Interdisciplinary Scientific Research in 2015, the Australian Academy of Science John Booker Medalist in 2017, and the Prime Minister's Malcolm McIntosh Prize for Physical Scientist of the Year 2017.

Mohsen Asadnia is a lecturer in the Engineering Department, Macquarie University. He received his Ph.D. in Mechanical Engineering from Nanyang Technological University (NTU)-Singapore and undertook his postdoctoral training at Singapore MIT Alliance for Research and Technology (SMART) and the University of Western Australia (UWA). His Ph.D. research was focused on the development of bio-inspired sensory systems using MEMS techniques. At MIT, he expanded his research inter-

est towards developing artificial inner ear haircell sensors. Dr. Asadnia is currently working on the development of novel transistor-based sensor technology for fast, reliable and accurate *in situ* monitoring of recycled wastewater. In addition, he is also collaborating with multi-disciplinary groups at Nanyang Technological University (NTU) and SMART for development of ultra-sensitive MEMS flow sensors for using in intravenous injections.

Majid E. Warkiani is a Senior Lecturer in the School of Biomedical Engineering, UTS, Sydney, Australia. He received his Ph.D. in Mechanical Engineering from Nanyang Technological University (NTU) and undertook postdoctoral training at Massachusetts Institute of Technology (SMART centre). He is also a member of Institute for Biomedical Materials & Devices (IBMD) and Center for Health Technologies (CHT) at UTS. Dr Warkiani's current research activities focus on three key areas of (i) Microfluidics involving the design and development of novel microfluidic systems for particle and cell sorting (e.g., circulating tumor cells, fetal cells & stem cells) for diagnostic and therapeutic applications, (ii) Bio-MEMS involving the fabrication and characterization of novel 3D lab-on-a-chip systems to model physiological functions of tissues and organs, and (iii) 3D Printing involving the design and development of novel miniaturized systems (e.g., micromixers, micro-cyclones) for basic and applied research.